Mesh-Based Shape Measurements with Stereocorrelation Principle and First Results

Lorène Dubreuil, John-Eric Dufour, Yann Quinsat, François Hild

XX manuscript No.
(will be inserted by the editor)

Mesh-Based Shape Measurements with Stereocorrelation

Principle and First Results

Lorène Dubreuil · John-Eric Dufour · Yann Quinsat · François Hild

Received: date / Accepted: date

Abstract A mesh-based framework is developed by extending global stereocorrelation techniques to faceted surfaces with three-noded elements. A two-step self-calibration procedure is followed to determine the projection matrices of the stereo-rig and to update the nominal surface model to match the surface of interest. To prove the feasibility of mesh-based stereocorrelation, two different test parts are analyzed with the present techniques and compared to already validated optical procedures.

Keywords Calibration · DIC · finite element discretization · photogrammetry · stereocorrelation

1 Introduction

Geometries of manufactured parts are designed to fulfil functional requirements such as assembly constraints and fatigue life. It is therefore essential to directly control the manufacturing process.

L. Dubreuil, Y. Quinsat
LURPA, ENS Cachan, Univ. Paris-Sud, Université Paris-Saclay,
94235 Cachan, France
E-mail: yann.quinsat@lurpa.ens-cachan.fr

J.-E. Dufour, F. Hild
LMT-Cachan, ENS Cachan / CNRS / Univ. Paris-Saclay
61 avenue du Président Wilson F-94235 Cachan Cedex, France

An additional procedure is to measure the actual geometry to evaluate its distance with respect to its nominal model. Several authors have proposed classifications of measurement systems [31,24, 30,9,29,1,39] to achieve such goals. Among them, contactless 3D shape reconstructions are one possible route in the field of metrology. One of their advantages is related to the fact that these techniques are often faster than conventional ones (*e.g.,* touch probe by employing coordinate measuring machines).

The most utilized contactless techniques are optical systems such as laser-plane sensor, fringe projection, photogrammetry, and stereovision. So-called stereocorrelation (or 3D surface digital image correlation (DIC) or stereo-DIC) is a method that allows 3D shapes *and* 3D displacements to be measured [20,35,21]. Clouds of 3D points and their motions are determined by analyzing various pairs of pictures. The metrological characterization of the observed surfaces then consists of post-processing the cloud of 3D points to determine the distance to the theoretical surface (*i.e.,* frequently the CAD model) by using, for instance, iterative closest point registration [4,6,37,19].

All the measurement techniques listed above require a calibration procedure to be performed. For stereoscopic systems (*e.g.,* stereovision, photogrammetry, stereocorrelation), the intrinsic and extrinsic parameters have to be determined [16,23,5]. A calibration target is generally used and several image pairs are shot for different positions of the target. An alternative route consists of using the observed part as the calibration target. Consequently, no calibration object is needed [17, 18]. Self-calibration aims to find intrinsic and extrinsic parameters of the stereo-rig directly from the pictures of the object of interest *itself*.

To perform such calibration, the mathematical description of the analyzed surface is needed. In that sense, the self-calibration procedures belong to the group of dense multiview methods [32]. The surface description can be based upon facets utilizing, say, Delaunay triangulation [36]. Freeform surface descriptions are also natural for global approaches to stereocorrelation [2]. In the following, finite element based surface descriptions will be used. They are based upon 3-noded

triangles (*i.e.,* T3 meshes). It is worth noting that other types of elements (*e.g.,* 4-noded quadrilaterals [14]) can also be considered within the very same framework. One advantage of such descriptions is that it provides direct and seamless links with finite element simulations [33,34].

The present paper is a follow-up on NURBS-based stereocorrelation [2]. Classical deviations experienced in manufacturing engineering cannot always be described with Non Uniform Rational B-Splines (NURBS [26]). These defects may be detected with the correlation residuals [13] but not easily quantified since they are continuous but not differentiable (*e.g.,* mismatches on surfaces manufacturing with different tools, roughness, scallop heights, facets). Conversely, with a faceted 3D shape, some of these geometrical defects may be detected *and* quantified. The work proposed herein consists of the implementation of mesh-based calibration and 3D shape measurements with T3 meshes.

The paper is organized as follows. In a first part, the mesh-based stereocorrelation method is presented and applied to a case study. Then this measurement is compared to a CAD-based approach. Advantages and drawbacks of both methods are mentioned. Finally, a feasibility study on a machined part is carried out to evaluate the ability of the proposed approach to detect machining defect.

2 Principle of Mesh-Based Stereocorrelation

In this section, the measurement of 3D shapes is carried out when its mathematical description is based upon finite elements. In the present case, three-noded triangular elements define facets of the surface model. In a finite element framework, facets only assume the continuity of the surface but not its first order derivatives, which may account for complex shapes (*e.g.,* mismatches, scallop heights induced by manufacturing).

The flow diagram shown in Figure 1 summarizes the different steps of the present implementation, which is a self-calibration procedure following the same steps as for isogeometric stereocorre-

lation [2]. The starting point of the analysis is the mathematical model of the observed shape and the pictures acquired by the left and right cameras. To initialize the stereocorrelation procedure, the user has to pick 6 remarkable points on the pictures and on the mesh. This allows for a first determination of the projection matrices that are needed to get the 2D positions in camera plane of a considered 3D point. In the present setting, the reference frame becomes that of the T3 mesh. The projection matrices are then updated by using an integrated approach to stereocorrelation. Once the calibration has been performed with the nominal mesh, the latter is updated to fit as best as possible the actual 3D shape. If needed these two last steps are repeated. In the present cases only one iteration was performed.

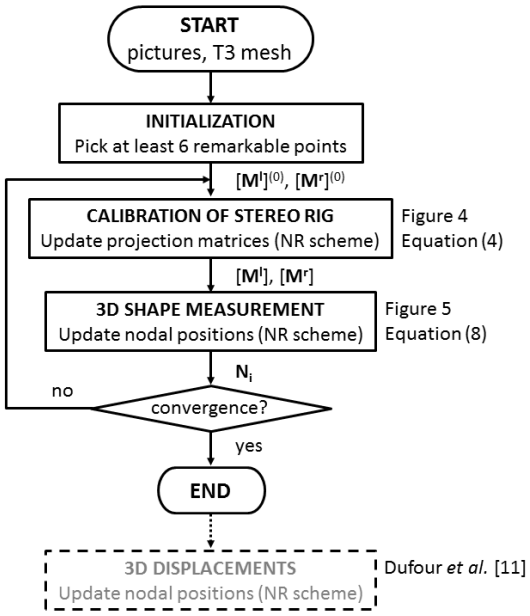

Fig. 1: Flow diagram of mesh-based stereocorrelation

Once the 3D shape has been measured, it may undergo displacements due to mechanical loading. The formalism proposed in Ref. [11,12] is applicable to the present parameterization. It

will not be followed hereafter since the aim of the paper is to show the feasibility of the present framework for 3D shape measurements and the detection of fabrication defects.

2.1 Surface Model

The mesh is assumed to be composed of nodes used to define facets. The facets are described with 3 nodes and a constant normal vector to get a triangular tessellation. This type of definition is classically considered in the Standard Tessellation Language (STL) format, which is widely used for rapid prototyping and computer-aided design and manufacturing [7]. Figure 2 shows an example of a CAD model using NURBS that is subsequently transformed into a mesh made of three-noded facets, which can be saved as a `.stl` file. It corresponds to the first test part used later on. The faceted 3D shape has been generated thanks to Catia V5 software [10]. In the present case, a quasi uniform T3 mesh is obtained since the 3D shape is not too complex.

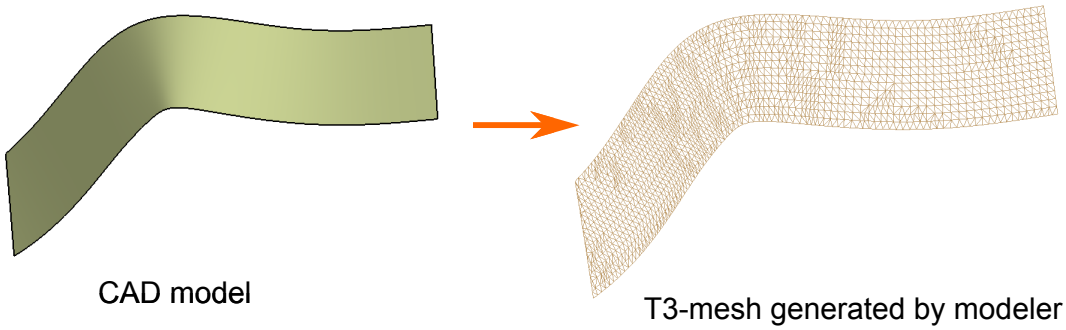

Fig. 2: NURBS-based CAD model of the first analyzed part (a) and corresponding `STL` model (b) generated by Catia V5 modeler

With the chosen parameterization of the observed surface, the unknowns are the positions of the nodes of the mesh, provided the stereo-rig has been calibrated. This is the first step of the present procedure.

2.2 Calibration of Stereovision System

The calibration of a stereo rig consists of determining the intrinsic parameters (*i.e.,* internal parameters of each camera), and the extrinsic parameters (*i.e.,* orientation and position of each camera with respect to a reference frame) [15,35]. All these parameters are used to define the so-called projection matrices $[\boldsymbol{M}^l]$ and $[\boldsymbol{M}^r]$, which relate the homogeneous coordinates $\{\boldsymbol{X}\}$ of any point in the scene of observation to the homogeneous coordinates of their respective projections onto the left $\{\boldsymbol{x}^l\}$ and right $\{\boldsymbol{x}^r\}$ cameras (Figure 3)

$$\left\{\begin{array}{c} s^l x^l \\ s^l y^l \\ s^l \end{array}\right\} = \Big[\boldsymbol{M}^l\Big] \left\{\begin{array}{c} X \\ Y \\ Z \\ 1 \end{array}\right\} \text{ and } \left\{\begin{array}{c} s^r x^r \\ s^r y^r \\ s^r \end{array}\right\} = \Big[\boldsymbol{M}^r\Big] \left\{\begin{array}{c} X \\ Y \\ Z \\ 1 \end{array}\right\} \tag{1}$$

where X, Y, Z are the three coordinates of the considered point, s^l, s^r the scale factors associated with the left and right imaging systems. It follows that for any 2D spatial parametrization u, v of the external surface, the coordinates $\boldsymbol{x}^l$ and $\boldsymbol{x}^r$ in the left and right cameras read

$$\boldsymbol{x}^l = \boldsymbol{x}^l(u, v, [\boldsymbol{M}^l]) \quad , \quad \boldsymbol{x}^r = \boldsymbol{x}^r(u, v, [\boldsymbol{M}^r]) \tag{2}$$

The projection matrices are determined by assuming that the observed surface corresponds to its nominal definition (*i.e.,* the T3 mesh generated by the CAD modeler). It is a self-calibration procedure in which no special target is needed (Figure 4). An integrated approach to stereocorrelation is followed as already proposed for NURBS-based descriptions of the observed surface [2]. The underlying minimization principle is based upon the conservation of the gray level in pictures f^l, f^r shot by the left and right cameras

$$f^l(\boldsymbol{x}^l) = f^r(\boldsymbol{x}^r) \tag{3}$$

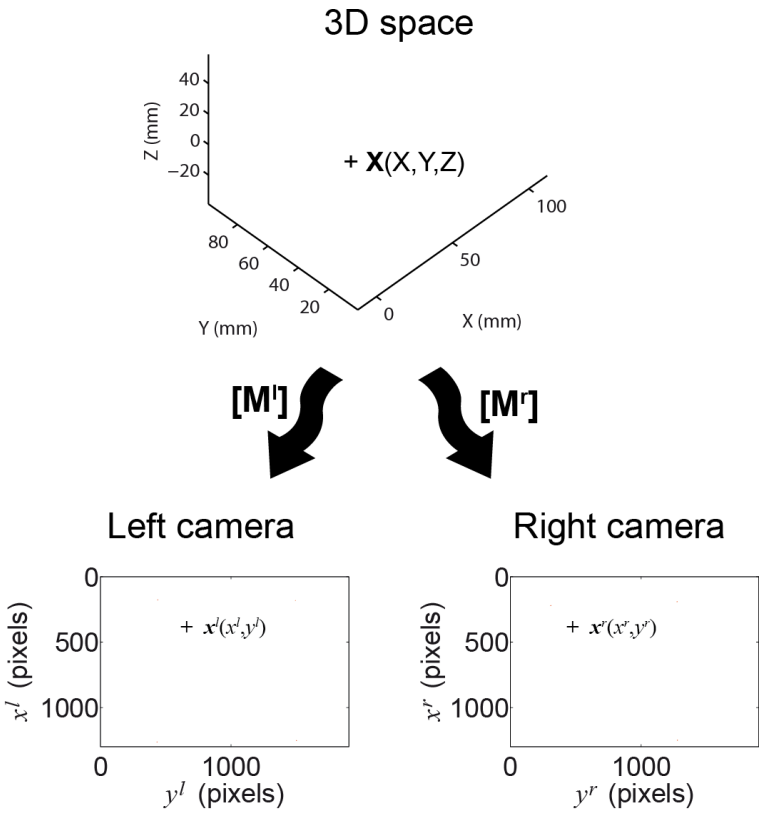

Fig. 3: Depiction of projections from 3D points in a scene observed by a stereosystem consisting of two cameras

which is globally minimized over the region of interest (ROI) with respect to the unknown components of the projection matrices

$$[\boldsymbol{M}^l], [\boldsymbol{M}^l] = \underset{[\boldsymbol{\mu}^l],[\boldsymbol{\mu}^r]}{\arg\min} \sum_{ROI} \Big(f^l(\boldsymbol{x}^l(u,v,[\boldsymbol{\mu}^l])) - f^r(\boldsymbol{x}^r(u,v,[\boldsymbol{\mu}^r])) \Big)^2 \tag{4}$$

This minimization is performed via a modified Newton-Raphson scheme for which the argument of the previous functional is successively linearized and corrected by evaluating the corrections (gathered in vectors $\{\delta\boldsymbol{\mu}^l\}$ and $\{\delta\boldsymbol{\mu}^r\}$) to the current estimate of the projection matrices $[\boldsymbol{\mu}^l]$ and $[\boldsymbol{\mu}^r]$

$$\tau_{lin} = \sum_{ROI} \left(f^l(\boldsymbol{x}^l) + [\boldsymbol{G}^l](\boldsymbol{x}^l)\{\delta\boldsymbol{\mu}^l\} - f^r(\boldsymbol{x}^r) - [\boldsymbol{G}^r](\boldsymbol{x}^r)\{\delta[\boldsymbol{\mu}^r\} \right)^2 \tag{5}$$

with

$$G^l_{ij}(\boldsymbol{x}^l) = \left(\boldsymbol{\nabla} f^l \cdot \frac{\partial \boldsymbol{x}^l}{\partial \mu^l_{ij}} \right)(\boldsymbol{x}^l) \quad , \quad G^r_{ij}(\boldsymbol{x}^r) = \left(\boldsymbol{\nabla} f^r \cdot \frac{\partial \boldsymbol{x}^r}{\partial \mu^r_{ij}} \right)(\boldsymbol{x}^r) \tag{6}$$

where the dependence of $\boldsymbol{x}^l$ and $\boldsymbol{x}^r$ with $u, u, [\boldsymbol{\mu}^l], [\boldsymbol{\mu}^r]$ has been omitted for the sake of clarity. Any changes to the projection matrices update the left and right coordinates according to Equation (2). Even though the minimization is based upon a quadratic approximation of the functional (4), the gray level residuals $\rho(u,v) = f^l(\boldsymbol{x}^l(u,v,[\boldsymbol{\mu}^l])) - f^r(\boldsymbol{x}^r(u,v,[\boldsymbol{\mu}^r]))$ are evaluated by accounting for all non linearities.

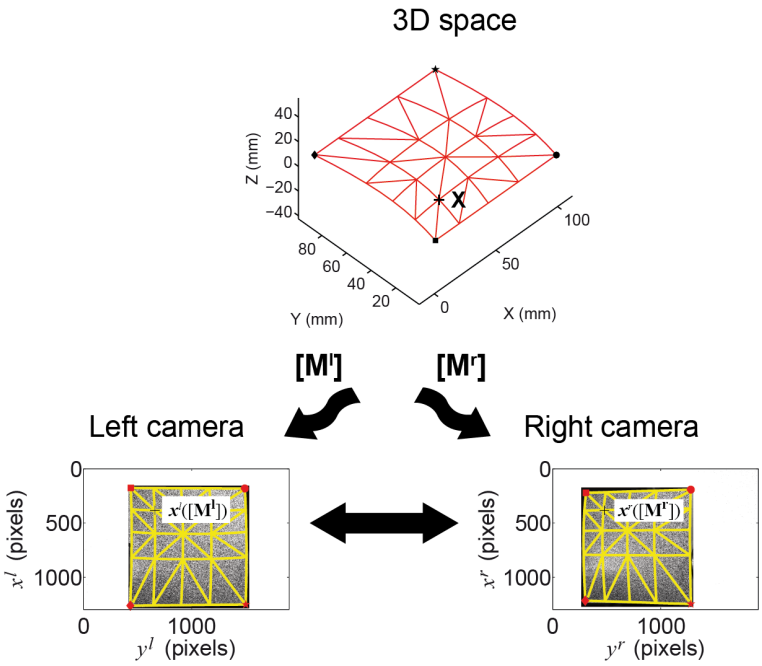

Fig. 4: Calibration step based upon surface tessellation using T3 facets

To initialize the calibration procedure, a first estimate $\boldsymbol{x}^l_0(u,v,[\boldsymbol{\mu}^l_0]), \boldsymbol{x}^r_0(u,v,[\boldsymbol{\mu}^r_0])$ is needed. Six points are selected by the user on each picture and on the nominal (*i.e.,* theoretical) surface.

By inverting system (1) in the least squares sense, initial values $[\boldsymbol{\mu}_0^l]$ and $[\boldsymbol{\mu}_0^r]$ for the projection matrices are obtained. The updated projection matrices are then determined by minimizing τ_{lin} with respect to $\delta[\boldsymbol{\mu}^l]$ and $\delta[\boldsymbol{\mu}^r]$. Once the previous corrections reach levels that are very low (*i.e.,* typically of the order of 10^{-3}), the iterations are stopped. The quality of the registration (and therefore of the calibration) is checked by computing the correlation residuals ρ for *all* the considered estimation points u, v in the ROI.

After this first step, the stereoscopic system has been calibrated. The next step consists of adapting the T3 mesh to the actual surface.

2.3 3D Shape Measurement

In this section, the T3 mesh is deformed to match the real surface of interest. As the surface is faceted, the deformation consists of moving the nodes of the tessellation to minimize the correlation residuals. In the present case, the initial and deformed meshes have exactly the same structure. Consequently, the nodal coordinates become the new unknowns to the correlation procedure. Their position is updated by using the same type of correlation procedure as previously described. The coordinates $\boldsymbol{x}^l$ and $\boldsymbol{x}^r$ in the left and right cameras are now written as functions of the nodal coordinates $\boldsymbol{N_i}$ of the T3 mesh (Figure 5)

$$\boldsymbol{x}^l = \boldsymbol{x}^l(u, v, \boldsymbol{N_i}) \quad , \quad \boldsymbol{x}^r = \boldsymbol{x}^r(u, v, \boldsymbol{N_i}) \tag{7}$$

The nodal positions are determined by globally minimizing over the region of interest (ROI)

$$\boldsymbol{N_i} = \underset{\boldsymbol{\nu_i}}{\arg\min} \sum_{ROI} \Big(f^l(\boldsymbol{x}^l(u, v, \boldsymbol{\nu_i})) - f^r(\boldsymbol{x}^r(u, v, \boldsymbol{\nu_i})) \Big)^2 \tag{8}$$

with respect to the unknown positions $\boldsymbol{\nu_i}$.

In the present case, the initial nodal positions are those in the nominal model since the calibration step has allowed the frame of the model to be related to that of the stereo rig. In order to leave the mesh structure unaltered, nodes from their initial positions are moved along their

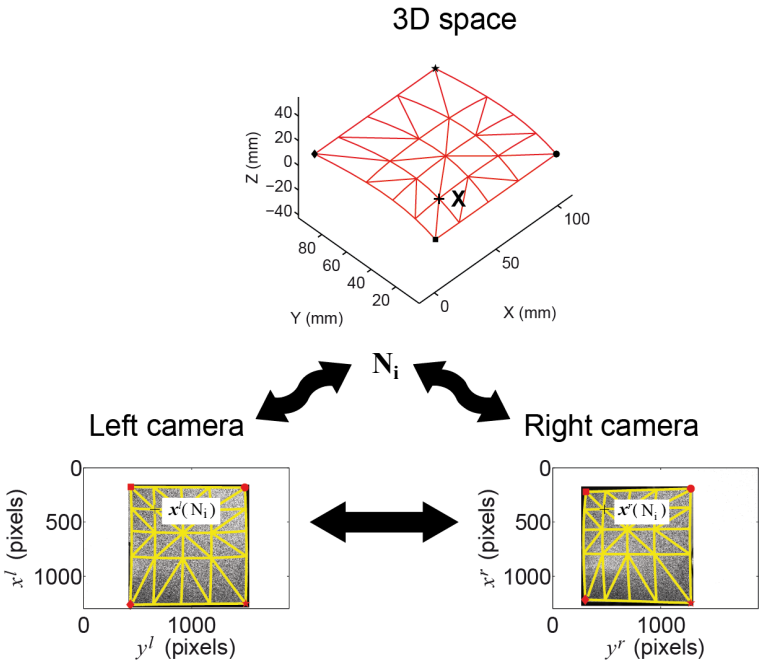

Fig. 5: 3D shape measurement based upon surface tessellation with 3D facets

normals only (Figure 6). This type of regularization is needed to avoid distorting T3 facets or even having interpenetrating points. Figure 7 depicts the initial and final surfaces whose nodes have undergone displacements along their normals (green arrows). The red arrows depict unwanted displacements. Once the nodes have been moved, the normals are not updated since it is assumed that only minute corrections are needed. This hypothesis was checked *a posteriori* in the following analysis.

With displacements following the normal of each node, the number of unknowns is divided by 3. However, the normal for each node has to be evaluated. By construction, the normals to the facets are readily available. The normal of a node is given by the weighted average of the normals to the facets that are connected to it. Since the element size was approximately identical, the weighted average is approximated by the mere vector average.

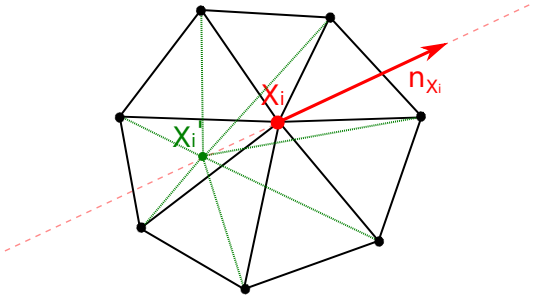

Fig. 6: Principle of node displacement along its normal

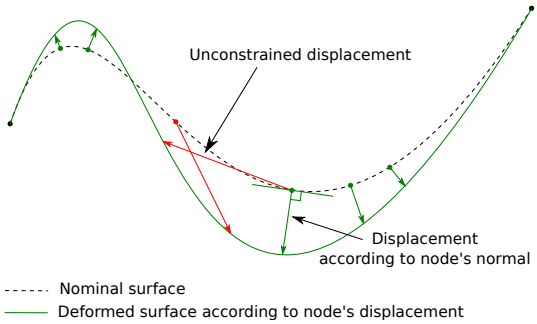

Fig. 7: Principle of node displacement along its normal for a node all its normal direction (reference configuration in black, deformed configuration in green)

In the case of surface models based upon tessellations, the unknowns are nodal coordinates. However, the minimization is performed over a significantly larger number of points to make the inversion of the registration problem possible. Consequently, the evaluation points u, v are to be defined for each facet. They would correspond to the integration points in standard finite element procedures [38]. Because the picture gradients have complex fluctuations, no standard quadrature (*e.g.,* Gauss points) is used. A uniform distribution of evaluation points is defined in each facet. Once the evaluation points have been defined, their respective positions in the left and right cameras are given by Equation (1). The corresponding gray level and local gradients are obtained through linear interpolations at inter-pixel locations. Figure 8 exemplifies this sub-element discretization using 6×6 evaluation points. This number was choose according to the

number of pixels contained in the projected mesh's face. Greater discretization may be performed in the case of a larger mesh size or a better image resolution.

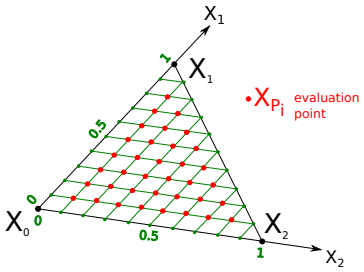

Fig. 8: Discretization of a T3 facet with 36 evaluation points

2.4 Results on Smooth Surface

The previous procedure has been tested on a T3-mesh shown in Figure 2. Several residual maps at different stages of the global optimization are reported in Figure 9. The first map refers to the stereocorrelation residual for the initial estimate of the projection matrix once the six points have been manually selected. Only a crude estimate is obtained since high levels are still observed. The second map corresponds to the stereocorrelation residuals after the calibration step. A clear gain is observed thanks to the fine repositioning of the cameras (*i.e.,* updating the projection matrices). The last map shows the stereocorrelation residuals when the optimization of the T3-mesh (*i.e.,* moving the nodes) is performed. There is a significant gain that indicates that the nominal nodal positions had to be corrected. At the end of this step, the measured 3D shape is directly expressed in terms of its mathematical description in the frame of the original model. The distance to the initial model is evaluated in a straight forward manner since the motions of all nodes are actually measured.

Following this study on the T3-mesh model surface, the map of deviations between the nominal T3-mesh (Figure 2) and the updated T3-mesh is shown in Figure 10. They correspond to the nodal

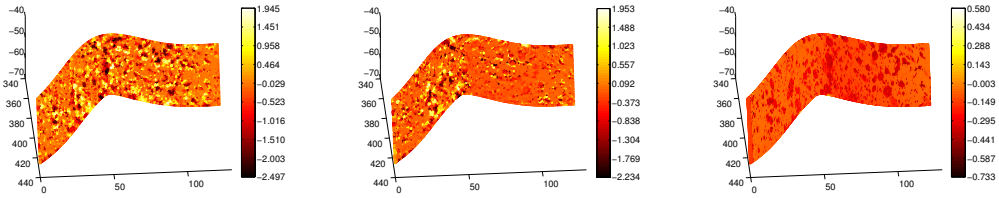

(a) Initial residual (b) Calibration step (c) 3D shape measurement

Fig. 9: Stereocorrelation residuals (expressed in a logarithmic mapping of the grey level intensity) at different steps of the procedure

motions that had to be applied to minimize the stereocorrelation residuals. A mean deviation of 77 μm is found and a standard deviation of 66 μm is obtained highlighting that most of the displacements are very small, thereby indicating that the machined shape is very close to the nominal model. It is worth noting that a part of the deviation and fluctuations is related to the paint. In the present cases, the mean thickness of the paint, which was determined by using a chromatic confocal sensor, is of the order of 40 μm, and its RMS roughness is less than 5 μm. Consequently, about half of the deviation is caused by the paint. Conversely, most of the observed fluctuations are not related to the paint but on the measurement uncertainties and on the fabrication process itself.

3 Comparison with CAD-Based Stereocorrelation

3.1 Isogeometric Stereocorrelation

The following approach is based on a NURBS description of the surface [2]. It is defined by its order, a network of control points $\boldsymbol{P}_{ij}$ with associated weights ω_{ij}, and its knot vector. Any point $\boldsymbol{X}$ belonging to the considered surface is expressed via two parameters $(u^*, v^*) \in [0,1]^2$

$$\boldsymbol{X}(u^*, v^*) = \frac{\sum_{i=0}^{m} \sum_{0=1}^{n} N_{ip}(u^*) N_{jq}(v^*) w_{ij} \boldsymbol{P}_{ij}}{\sum_{i=0}^{m} \sum_{0=1}^{n} N_{ip}(u^*) N_{jq}(v^*) w_{ij}} \tag{9}$$

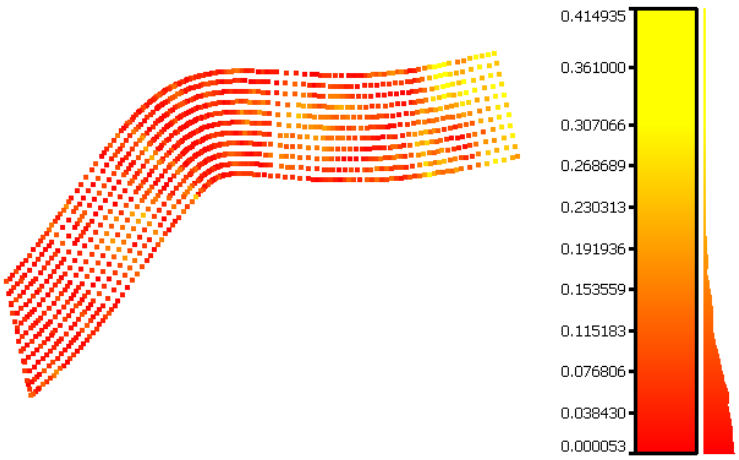

Fig. 10: Deviation map (expressed in mm) between the nominal model and the updated T3-mesh measured via global stereocorrelation

where N_{ip} are the mixing functions [26]. Instead of updating the nodal positions, isogeometric stereocorrelation consists of moving the control points that deform the nominal surface to match as best as possible the actual geometry. The pseudo displacements in the left and right pictures then read

$$\delta x^{l,r} = \frac{\partial x^{l,r}}{\partial X} \frac{\partial X}{\partial \boldsymbol{P}_{ij}} d\boldsymbol{P}_{ij} \tag{10}$$

CAD-based (or isogeometric stereocorrelation [2] follows similar steps as those proposed herein for mesh-based stereocorrelation (Figure 1) since both are based upon self-calibration. First, an initialization step is required to have a first estimate of the projection matrices. The latter ones are then updated by using the same functional (4). Last, the NURBS model is updated by moving its control points to minimize the sum of squared differences between the gray levels of left and right pictures over all considered evaluation points instead of the nodal positions for mesh-based stereocorrelation. The main difference between the two methods thus lies in the mathematical model of the analyzed 3D shape. The interested reader will find additional details on isogeometric stereocorrelation in Refs. [2, 12].

Table 1 shows the difference in terms of degrees of freedom and interpolation degree of the initial CAD model when using NURBS and its STL definition. The NURBS description generally has very few knots (*i.e.,* control points) in comparison with the number of nodes of the corresponding T3 tessellation (Figure 2).

Table 1: Model parameters description

Type of model	number of nodes (or knots)	maximum interpolation degree
NURBS model	68	8
T3 model	1370	1

3.2 Results

The deviations of the measured NURBS surface with respect to its nominal model (Figure 2) are shown in Figure 11. A mean deviation of 36 μm and a standard deviation of 27μm are obtained. The present result shows smaller deviations from the nominal model than those measured with the previous method. The present deviations are mainly due to small oscillations observed on the deformed NURBS surface. This phenomenon appears essentially in the center of the surface and results from a high number of control points and degrees used to describe the surface. Even though the present implementation was not regularized [13] the fact that a very small number of control points is used in comparison with the T3-mesh (Table 1) is advantageous for the NURBS-based approach. In the present case, the NURBS-approach out-performs the mesh based approach. However, the latter yields results that are close to the former, thereby validating its implementation and the regularization strategy consisting of moving nodes along their normal direction only.

Two measurement methods based on a CAD model have been described in this section. As the number of parameters (control points, weights, nodal sequence) necessary to describe NURBS

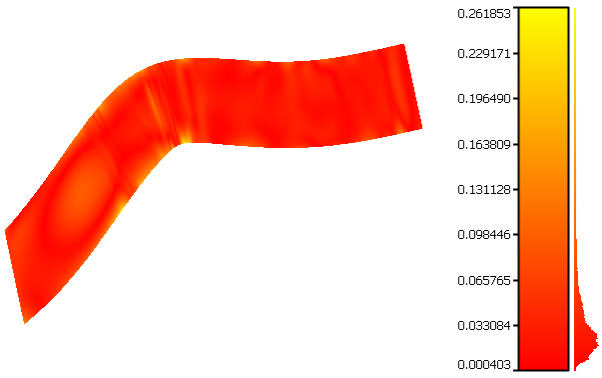

Fig. 11: Deviations (expressed in mm) between the theoretical model and the reconstructed 3D shape

surfaces compared to a tessellation representation is lower, the NURBS-based method is easier to implement. However, the NURBS representation does not allow geometric features with tangent and curvature discontinuity to be described. Moreover, local variations encountered in machining processes (*e.g.,* mismatches, scallop heights, facets) are very difficult to model in a NURBS formalism. In these cases, the mesh-based method presented in this section may be more efficient since deformations can be performed more locally.

4 Application to Defect Detection

To illustrate the relevance of the proposed method for machining defect detection, a second test part is analyzed. Two different measuring systems are used to assess deviations induced by machining. The first system consists of a coordinate measuring machine (*i.e.,* CMM) equipped with a laser-plane sensor (Kreon) mounted on an orientation head to increase the sensor resolution. The second technique is mesh-based stereocorrelation.

The studied deviations are those obtained during milling of a complex shape (*e.g.,* mismatches, scallop heights, facets). The CAD model of the studied part is shown in Figure 12. This part has three different types of defects. It has been machined via the so-called parallel plane strategy. Thus,

all the tool paths are aligned along the same machining direction. Some defects, such as facets, are machined on purpose and described in the nominal model. Mismatch and scallop heights will also occur during machining.

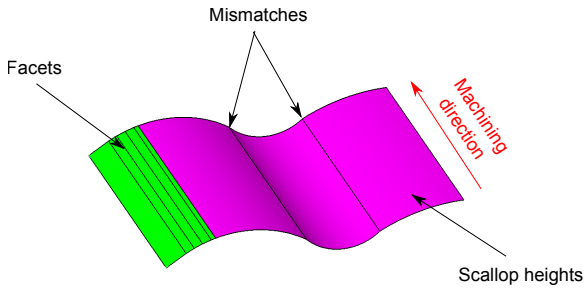

Fig. 12: CAD model of the studied part

4.1 Laser-Plane Sensor

This first system has been chosen to scan the surface with only one orientation of the laser in order to avoid overlapping errors generally appearing when using multiple sensor orientations and to reduce deviations due to orientation changes [3]. Based on the iterative closest point algorithm an interpolation of the digitized point cloud is performed. It is worth remembering that this operation is directly performed with the proposed stereocorrelation procedure (*i.e.,* first calibration step).

The results are given in Figure 13 in terms of the deviations between the CAD model and the measured point cloud. The standard deviation and mean offset are respectively equal to 79 μm and 22 μm. To illustrate the type of encountered deviation, a section is extracted in a plane orthogonal to the machining direction. From this section, mismatches are easily identified in the present case contrary to scallop heights, which are not detected. Following this measurement, only the mismatch is quantified with this measuring system. With such a system, it is not possible to

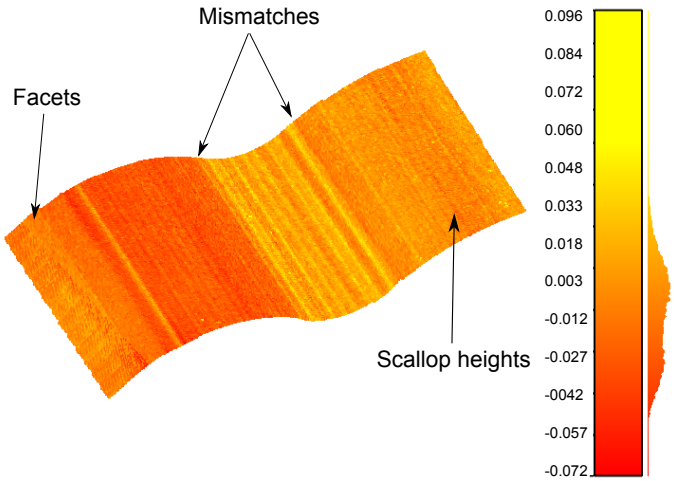

Fig. 13: Deviations (expressed in mm) between the nominal model and the laser-plane sensor digitization

quantify the value of the scallop height and the facets are difficult to analyze. This is due to the resolution of the present system [39].

4.2 Mesh-Based Stereocorrelation

The part is also measured with the mesh-based stereocorrelation method introduced in Section 2. To perform mesh-based stereocorrelation, two pictures are shot. Figure 14 shows that a random pattern using black and white paint has been sprayed to make such analyses possible. It is worth noting that this coating has been applied *after* the measurement with the laser-plane sensor.

The calibration of the stereoscopic system is carried out thanks to the T3-meshed surface. The mesh used herein is obtained from an output of the CAD software. Prior to the application of stereocorrelation, a visibility analysis [22] is performed to remove the mesh faces that cannot be seen by both cameras. The stereocorrelation residual following the first calibration step is shown in Figure 15(a). Areas with large residuals correspond to locations with a larger deviation in the measurement performed with the laser plane sensor. After optimization the residual is smaller

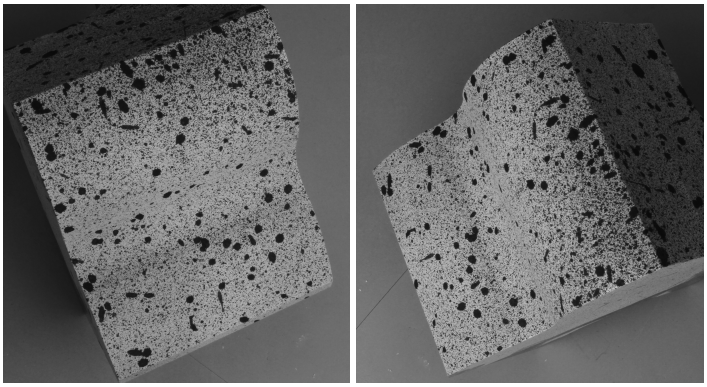

(a) (b)

Fig. 14: Left (a) and right (b) pictures of the analyzed part

in these areas (Figure 15(b)). Some areas have still large residuals indicating that the assumed shape is not necessarily compatible with the actual shape.

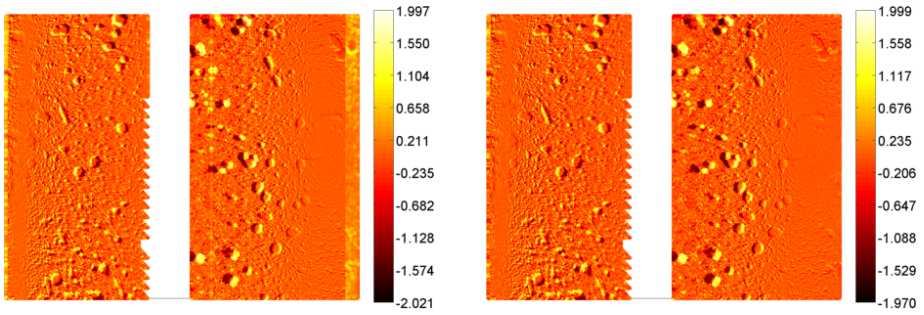

(a) (b)

Fig. 15: Stereocorrelation residual maps prior to (a) and after (b) surface corrections (expressed in a logarithmic mapping of the grey level intensity)

The measured offset field is shown in Figure 16. A mean deviation of 8.3 μm and a standard deviation of 8.8 μm are found. On the left side, two vertical stripes appear, which are illustrating the presence of a defect on the facets while the point cloud obtained with the laser-plane sensor does not allow this identification. On the right side the other two vertical stripes show that the

cylindrical section has undergone an overall horizontal motion illustrating the mismatch defect. However many nodes have very different offsets compared to their neighborhood. This is partly due to unsuitable (*i.e.,* too coarse) pattern in the measured area. These nodes are considered as outliers. With the chosen mesh size, the scallop height cannot be measured.

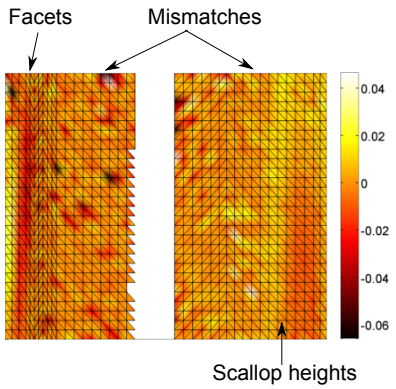

Fig. 16: Measured displacement along the normal direction to each node (expressed in mm)

In this section, the feasibility of mesh-based stereocorrelation to identify specific defects is studied. The study is carried out on a test part including classical defects encountered during milling (*i.e.,* mismatch, form error, scallop height). The mesh-based stereocorrelation performance is compared with a commonly used laser-plane sensor. The results of this comparative study shows that the measurement method proposed herein could have an ability to discriminate machining defects comparable to current non-contact measuring systems.

5 Conclusions

A mesh-based stereocorrelation procedure has been presented within a global framework of DIC. One of its features is to describe observed surfaces within a dense multiview methods [32]. In the present case, multi-faceted surfaces are modeled with 3-noded surface elements. Further, a self-calibration procedure is followed. It allows the measurement results to be directly expressed

in the frame of the virtual model. This step is achieved by calibrating the projection matrices of the stereo-rig.

Since a self-calibration procedure is followed, the actual shape of the surface of interest is determined by directly updating its *a priori* definition. To avoid ill-conditioning of the stereocorrelation procedure, the 3D shape is updated by keeping the general structure of the mesh, namely, the nodes are only moved along the surface normals. It is worth noting that other regularization techniques may be followed when measuring 3D shapes and/or 3D surface displacement fields [27, 12, 13].

Two test cases have been studied to prove the feasibility of the previous framework to measure 3D shapes and to compare with existing procedures. The first tool is NURBS-based stereocorrelation that has already been validated by studying different cases [2, 11]. The second system is a laser-plane sensor that is mounted on a head of a coordinate measuring machine.

Compared to NURBS-based stereocorrelation, the proposed method increases the computation time due to the larger number of degrees of freedom of the surface representation. Yet it allows the measurement of more complex features to be performed that induce local deformations of the mesh such as machining defects. For the test part that was measured with the two stereocorrelation techniques, the overall results are consistent with each other, thereby validating the mesh-based approach proposed herein.

The measurements made with laser-plane sensor and mesh-based stereocorrelation show the ability of the proposed method to detect local defects, which were not detected with the laser-plane sensor. In the context of surface inspection, it is necessary to compare the actual surface to its CAD definition. Hence, the point cloud obtained from contactless sensors such as the laser scanner must be brought back to the frame of the the CAD model. This step can be relatively long and difficult. A direct measurement in the frame of the virtual model as proposed with global stereocorrelation techniques eliminates this operation and the associated uncertainty.

In the present analysis, the defects could be detected yet not necessarily quantified. This last step would have required the T3 mesh to be compatible with the geometry of the defect(s). In Some cases, this may be possible. An alternative route would be to tailor patches associated with known defect geometries. This type of concept was used to detect and quantify multiple cracks in fatigue test [28].

Last, it is worth noting that from the virtual design of a structure to its (virtual) sizing different bridges are needed. For instance, surface tessellations can be obtained from CAD modelers [7, 10]. These faceted surfaces are useful data for finite element codes. Another alternative is to perform isogeometric analyses [8]. In both cases bridges with experimental procedures are desirable for identification and validation purposes. The present developments contribute to unify experiments and simulations so that the emergence of "simulation-based engineering sciences" will be facilitated [25].

References

1. B.R. Barbero and E. Santos Ureta. Comparative study of different digitization techniques and their accuracy. *Comput.-Aided Des.*, 43(2):188 – 206, 2011.
2. B. Beaubier, J.E. Dufour, F. Hild, S. Roux, S. Lavernhe-Taillard, and K. Lavernhe-Taillard. CAD-based calibration of a 3D-DIC system: Principle and application on test and industrial parts. *Exp. Mech.*, 54(3):329–341, 2014.
3. I. Bešić, N. Van Gestel, J.-P. Kruth, P. Bleys, and J. Hodolić. Accuracy improvement of laser line scanning for feature measurements on CMM. *Opt. Lasers Eng.*, 49(11):1274–1280, 2011.
4. P.J. Besl and N.D. McKay. A method for registration of 3-D shapes. *IEEE Trans. Patt. Anal. Mach. Intell.*, 14(2):239–256, 1992.
5. Jean-Yves Bouguet. Camera calibartion toolbox for matlab. 2010.
6. Y. Chen and G. Medioni. Object modelling by registration of multiple range images. *Image Vis. Comput.*, 10(3):145–155, 1992.
7. C.K. Chua, K.F. Leong, and C.S. Lim. *Rapid Prototyping: Principles and Applications (2nd ed.)*. World Scientific Publishing, 2003.
8. J.A. Cottrell, T.J.R. Hughes, and Y. Bazilevs. *Isogeometric Analysis: Toward Integration of CAD and FEA*. Wiley, 2009.

9. W. Cuypers, N. Van Gestel, A. Voet, J.-P. Kruth, J. Mingneau, and P. Bleys. Optical measurement techniques for mobile and large-scale dimensional metrology. *Opt. Lasers Eng.*, 47(3-4):292–300, 2009.
10. Dassault Systems. CATIA V5 R19, online documentation. http://www.3ds.com/products/catia/welcome/, 2008.
11. J.-E. Dufour, B. Beaubier, F. Hild, and S. Roux. CAD-based displacement measurements. Principle and first validations. *Exp. Mech.*, 55(9):1657–1668, 2015.
12. J.-E. Dufour, F. Hild, and S. Roux. Shape, Displacement and Mechanical Properties from Isogeometric Multiview Stereocorrelation. *J. Strain Analysis*, 50(7):470–487, 2015.
13. J.-E. Dufour, S. Leclercq, J. Schneider, F. Hild, and S. Roux. 3D surface measurements with isogeometric stereocorrelation. Application to complex shapes. *Opt. Lasers Eng.*, DOI: 10.1016/j.optlaseng.2016.02.018, 2016.
14. J.E. Dufour, B. Beaubier, S. Roux, and F. Hild. Displacement measurement using CAD-based stereocorrelation with meshes. In *ICEM conference proc.*, 2014.
15. O. Faugeras. *Three-dimensional computer vision: a geometric viewpoint.* MIT Press, Cambridge, MA (USA), 1993.
16. O Faugeras and G Toscani. Camera calibration for 3D computer vision. *International Workshop on Machine Vision and Machine Intelligence*, pages 240–247, 1987.
17. O.D. Faugeras, Q.T. Luong, and S.J. Maybank. Camera self-calibration: Theory and experiments. In *Proc. 2nd ECCV*, pages 321–334. Springer-Verlag, 1992.
18. A. Fusiello. Uncalibrated euclidean reconstruction: A review. *Im. vis. comput.*, 18:555–563, 2000.
19. J. Harvent, B. Coudrin, L. Brèthes, J.-J. Orteu, and M. Devy. Multi-view dense 3D modelling of untextured objects from a moving projector-cameras system. *Mach. Vis. Appl.*, 24(8):1645–1659, 2013.
20. J.D. Helm, S.R. McNeill, and M.A. Sutton. Improved three-dimensional image correlation for surface displacement measurement. *Opt. Eng.*, 35(7):1911–1920, 1996.
21. F. Hild and S. Roux. Digital image correlation. In P. Rastogi and E. (eds) Hack, editors, *Optical Methods for Solid Mechanics. A full-Fild Approach.* Wiley-VCH, Weinheim (Germany), 2012.
22. S. Katz, A. Tal, and R. Basri. Direct visibility of point sets. *ACM Trans. Graph.*, 26(3), 2007.
23. J.-M. Lavest, M. Viala, and M. Dhome. Quelle précision pour une mire d'étalonnage ? 1999.
24. Y. Li and P. Gu. Free-form surface inspection techniques state of the art review. *Comput.-Aided Des.*, 36(13):1395 – 1417, 2004.
25. Blue Ribbon Panel. Simulation-based engineering sciences. Final report, NFS (www.nsf.gov/pubs/reports/sbes_final_report.pdf), 2006.
26. L. Piegl and W. Tiller. *The NURBS Book.* Springer, 2nd edition, 1997.
27. J. Réthoré, Muhibullah, T. Elguedj, M. Coret, P. Chaudet, and A. Combescure. Robust identification of elasto-plastic constitutive law parameters from digital images using 3D kinematics. *Int. J. Solids Struct.*, 50(1):73–85, 2013.
28. J. Rupil, S. Roux, F. Hild, and L. Vincent. Fatigue microcrack detection with digital image correlation. *J. Strain Analysis*, 46(6):492–509, 2011.

29. G. Sansoni, M. Trebeschi, and F. Docchio. State-of-the-art and applications of 3D imaging sensors in industry, cultural heritage, medicine, and criminal investigation. *Sensors*, 9(1):568–601, 2009.
30. E. Savio, L. De Chiffre, and R. Schmitt. Metrology of freeform shaped parts. *CIRP Annals - Manufacturing Technology*, 56(2):810 – 835, 2007.
31. H. Schwenke, U. Neuschaefer-Rube, T. Pfeifer, and H. Kunzmann. Optical methods for dimensional metrology in production engineering. *CIRP Annals - Manufacturing Technology*, 51(2):685 – 699, 2002.
32. S.M. Seitz, B. Curless, J. Diebel, D. Scharstein, and R. Szeliski. A comparison and evaluation of multi-view stereo reconstruction algorithms. *Proc. IEEE Conf. Computer Vision and Pattern Recognition*, 1:519–526, 2006.
33. M.A. Sutton. Computer vision-based, noncontacting deformation measurements in mechanics: A generational transformation. *Appl. Mech. Rev.*, 65(AMR-13-1009, 050802), 2013.
34. M.A. Sutton and F. Hild. Recent advances and perspectives in digital image correlation. *Exp. Mech.*, 55(1):1–8, 2015.
35. M.A. Sutton, J.-J. Orteu, and H. Schreier. *Image Correlation for Shape, Motion and Deformation Measurements: Basic Concepts,Theory and Applications*. Springer Publishing Company, Incorporated, 2009.
36. H.H. Vu, P. Labatut, J.P. Pons, and R. Keriven. High accuracy and visibility-consistent dense multiview stereo. *IEEE Trans. Pattern Anal. Machine Intell.*, 34(5):889–901, 2012.
37. Z. Zhang. Iterative point matching for registration of free-form curves and surfaces. *Int. J. Comput. Vis.*, 13(2):119–152, 1994.
38. O.C. Zienkievicz and R.L. Taylor. *The Finite Element Method*. McGraw-Hill, London (UK), 4th edition, 1989.
39. A. Zuquete-Guarato, C. Mehdi-Souzani, Y. Quinsat, C. Lartigue, and L. Sabri. Towards a new concept of in-line crankshaft balancing by contact less measurement: process for selesction the best digitizing system. 2012.